JOURNAL OF PROPULSION AND POWER
Vol. 11, No. 1, January–February 1995

Atomization Characteristics of Impinging Liquid Jets

H. M. Ryan,* W. E. Anderson,† S. Pal,‡ and R. J. Santoro§
Pennsylvania State University, University Park, Pennsylvania 16802

The atomization characteristics of sheets formed by both laminar and turbulent impinging jets were experimentally studied as a function of flow and injector geometric parameters. In particular, sheet breakup length along the sheet centerline, distance between adjacent waves apparent on the sheet, and drop-size distributions were measured over a Weber number range between 350–6600 and a Reynolds number range between 2.8×10^3 to 2.6×10^4. A linear stability-based model was used to determine the most unstable wave number and the corresponding growth rate factor on two-dimensional thinning inviscid and viscous sheets. These wave characteristics were used to predict both the sheet breakup length and the resulting drop sizes. A second model, applicable for a low Weber number regime, in which sheet disintegration is controlled by stationary antisymmetric waves, was used to predict the shape of the sheet formed by two impinging liquid jets. The linear stability-based theory predictions of breakup length did not agree in trend or magnitude with experimental measurements. However, for Weber numbers less than 350, the measured breakup length for laminar impinging jets was within 50% of that predicted by the stationary antisymmetric wave-based model. Finally, drop-size predictions based on linear stability theory agreed in trend, but not in magnitude, with the measured drop sizes. The contrast between the sheet atomization characteristics of laminar vs turbulent impinging jets suggest that the initial conditions of the impinging jets significantly influence the sheet breakup mechanism. Also, the comparison between experimental results and theoretical predictions indicates that the impact wave generation process at the jet impingement point needs to be incorporated in the theoretical models for sheet atomization.

Nomenclature

d = diameter
F = thickness distribution
h = sheet thickness
k = wave number
L = length of injection element
l = length
r = radial distance from impingement point
Re = Reynolds number, $U_j d_o/\nu_l$, based on liquid properties, jet velocity, and orifice diameter
Re_s = Reynolds number, $U_s h/\nu_l$, based on liquid properties, sheet velocity, and sheet thickness
s = ratio of gas density to liquid density
t = time
U = velocity
W = maximum width of sheet
We = Weber number, $\rho_l U_j^2 d_o/\sigma$, based on liquid properties, jet velocity, and orifice diameter
We_s = Weber number, $\rho_l U_s^2 h/\sigma$, based on liquid properties, sheet velocity, and sheet thickness
x = axial distance from impingement point
y = coordinate perpendicular to x in the plane of the sheet
α = fan inclination angle
β = complex growth rate factor, $\beta_r + i\beta_i$
η = disturbance amplitude
θ = impingement half-angle
λ = wavelength
μ = dynamic viscosity
ν = kinematic viscosity
π = pi, 3.14159
ρ = density
σ = surface tension
ϕ = angular coordinate on sheet

Subscripts
b = breakup
D = drop
e = edge
g = gas
i = imaginary
j = jet
L = ligament
l = liquid
m = maximum
nd = nondimensional
o = orifice or initial
r = real
s = sheet
sw = surface wave
10 = arithmetic
30 = volume

Received Feb. 20, 1993; revision received April 12, 1994; accepted for publication April 27, 1994.

*Graduate Student, Propulsion Engineering Research Center, Department of Mechanical Engineering. Member AIAA.
†Graduate Student, Propulsion Engineering Research Center, Department of Mechanical Engineering.
‡Research Associate, Propulsion Engineering Research Center, Department of Mechanical Engineering. Member AIAA.
§Professor, Propulsion Engineering Research Center, Department of Mechanical Engineering. Member AIAA.

Introduction

IMPINGING jet injectors are commonly used in many rocket engines, prominent examples being the F-1, H-1, Titan, and XLR-132.[1] Furthermore, laser-drilled micro-orifice doublet impinging jet injectors have recently received attention due to their potential low cost and high efficiency.[2] Impinging jet injectors are most often used with RP-1/liquid oxygen (LOX) and nitrogen tetroxide (NTO)/monomethyl hydrazine (MMH) propellant combinations.[3] The relative ease of fabrication of impinging jet injectors also makes this type of injector an attractive alternative to coaxial injector elements typically used for LOX/H_2 engines. Currently, no mechanistic design analysis method exists for this common type of injector.

A schematic diagram of a typical like-on-like impinging jet injector and the resultant spray is shown in Fig. 1. The individual impinging jet injector elements are fed propellant through a manifold. The inlets are usually sharp-edged, there-

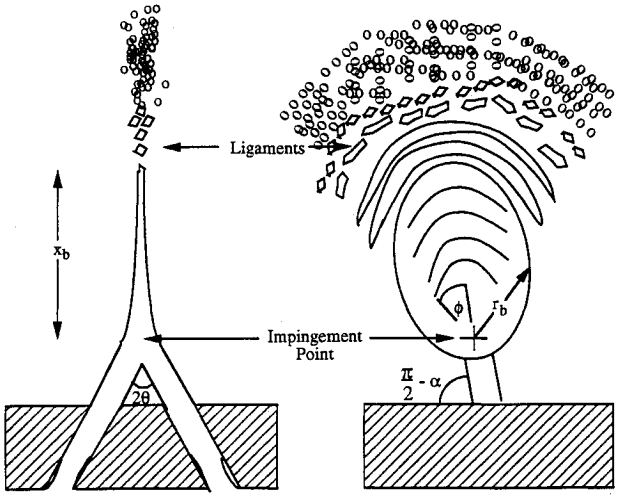

Fig. 1 Schematic diagram of a typical impinging jet spray.

fore, the flow detaches from the wall to form a vena contracta. The flow typically reattaches to the wall and exits into the chamber. The two emerging cylindrical jets impinge at a point with an impingement angle of 2θ, which is typically about 60 deg. *Re* and *We*, based on liquid properties, jet velocity, and orifice diameter, are on the order of 10^5–10^6 under rocket conditions. The length-to-diameter ratio L/d_o of the orifice, and the preimpingement length-to-orifice-diameter ratio l_i/d_o are both typically between 3–10. The symbol ϕ shown in Fig. 1 is the angular coordinate in the plane of the sheet. The impinging liquid jets form a sheet in a plane perpendicular to the plane of the jets, and the sheet is usually canted at an angle α from the normal to the injector faceplate to improve mixing.

The impetus behind understanding the atomization mechanism(s) of impinging jet injectors is the direct effect atomization has on subsequent combustion processes, and the established link between atomization and combustion instability phenomena.[1,3,4] Previous cold flow[4–8] and hot-fire[3] experimental studies of impinging jet atomization have typically involved changing the injector geometry and flow properties and recording the effect of these changes on the resultant spray. Visualizations of impinging jet sprays under both cold flow and hot-fire conditions indicate that the sheet breaks up in a periodic manner into ligaments, which subsequently disintegrate into drops.[3] Previous studies have shown that the sheet structure, ligament/drop formation frequency, and drop size are all sensitive to the injector design and operating parameters (e.g., Ref. 4). In addition, researchers have modeled the breakup behavior of impinging jets with varying degrees of complexity and success.[6–9] However, a fundamental understanding of the atomization mechanism(s) still does not exist.

In this study, measurements of sheet breakup length, and surface wave and periodic ligament separation characteristics made from instantaneous images of the impinging jet spray, and drop-size measurements within the spray field, are presented. These results are compared to predictions made with current modeling approaches, and with earlier experimental studies. Similar to previous workers,[5] the effects of laminar vs turbulent jet conditions on the spray breakup process have been studied over a Weber number range between 350–6600, and a Reynolds number range between 2.8×10^3 to 2.6×10^4. The objectives of the current study are to extend and confirm previous experimental work on impinging jet atomization and to provide a firm basis from which to address combustion instability phenomena associated with this type of injector. To aid in the comparison of current work with previous studies, a review of previous theoretical and experimental work on liquid sheet breakup is presented next.

Theoretical Models of Liquid Sheet Breakup

The study of atomization characteristics associated with many injector types often involves analyzing the breakup behavior of liquid sheets. There have been a number of theoretical studies of the general case of liquid sheet atomization,[10–20] as well as the atomization of a sheet formed by two impinging jets.[7–9] Models of liquid sheet atomization can be subdivided into numerical[10–12] and analytical treatments[13–20] based on the growth of infinitesimal disturbances due to aerodynamic stresses on the liquid sheet surface. The analytical models typically involve linear wave growth, whereas the numerical studies examine nonlinear wave growth. In a different approach, Childs and Mansour[10] used a Navier-Stokes method and a Lagrangian scheme to track the liquid-gas interface to provide an argument that boundary-layer effects in both the liquid and gas phases enhance the wave growth rate for wind-induced instabilities. These analytical and numerical studies provide insight into the important physical processes causing liquid sheet disintegration, and predict physical quantities, such as drop size, which compare relatively well with observations made in appropriate experimental studies. However, the application of linear and nonlinear wave growth based models to the case of sheets formed by two impinging jets has not been thoroughly investigated. Anderson et al.[8] adapted linear stability theory to the case of impinging jet atomization, whereas Ibrahim and Przekwas[9] extended Taylor's[7,19] work to predict the sheet shape at low Weber numbers. A review of linear stability theory for liquid sheet atomization applicable for high Weber number impinging jets, as well as Ibrahim and Przekwas'[9] sheet shape model for low Weber number impinging jets is discussed next.

Linear stability theory based on the growth of infinitesimal disturbances due to aerodynamic stresses on the liquid sheet surface has been used to describe the disintegration of liquid sheets.[13–18] The disturbance on the sheet surface η is given by

$$(\eta/\eta_o) = e^{\beta_i t} \tag{1}$$

where η_o is the initial displacement amplitude and β_i is the growth rate.

Typically, β_i is calculated for a spectrum of k. The disturbance wave number k_m corresponding to the maximum growth rate $\beta_{i,m}$, controls the breakup process. Both sinuous (antisymmetric) and dilatational (symmetric) waves can grow; however, previous research indicates that sinuous waves grow faster than dilatational waves,[13] hence, only the behavior of sinuous disturbances are considered hereafter. The theory does not predict a critical disturbance amplitude for sheet disintegration, and consequently, an empirical relation of the following form is used[14]:

$$\int_0^{t_b} \beta_{i,m}\, \mathrm{d}t = \int_0^{x_b} \frac{\beta_{i,m}}{U_s}\, \mathrm{d}x = 12 \tag{2}$$

where t_b is the sheet breakup time, x_b is the breakup distance, and U_s is the sheet velocity. Thus, through the above empirical equation, the length of the intact sheet can be determined once a relation for $\beta_{i,m}$ is ascertained. k_m associated with the fastest growing disturbance is used to subsequently predict the size of ligaments and drops shedding from the edge of the intact sheet.[14]

The derivation of an expression for the growth rate factor and the wave number has been done for an inviscid constant thickness sheet,[13] and an attenuating viscous sheet.[14,15] Other researchers have extended these equations describing sheet breakup to the case of the sheets formed by impinging jets.[8,9] A concise summary of the appropriate equations and their underlying assumptions is given next.

Squire[13] investigated the growth of antisymmetric disturbances for constant thickness, inviscid liquid films, and de-

rived expressions for the wave number and corresponding growth rate coefficient for the most unstable wave. k_m for the most unstable wave was given as

$$k_m = (\rho_g U_s^2/2\sigma) \tag{3}$$

where ρ_g is the gas density. The corresponding maximum growth rate factor was given by

$$\beta_{i,m} = (\rho_g U_s^2/\sqrt{2\rho_l \sigma h}) \tag{4}$$

The above two relations are valid for We_s $(=\rho_l U_s^2 h/\sigma) > 1$, and for disturbance wavelengths large compared to the sheet thickness. Squire[13] compared his predictions of the wavelength of the most unstable disturbance, λ_m $(=2\pi/k_m)$, to those measured from photographs of liquid sheets produced by a nozzle, and showed, in general, good agreement.

Dombrowski and Johns[14] extended Squire's[13] analysis by including the effects of viscosity and a diminishing sheet thickness in analyzing the disintegration of two-dimensional liquid sheets through aerodynamic instability. By considering a force balance on the liquid between pressure, surface tension, viscous, and inertial forces, they developed an equation relating the disturbance wave number and the growth rate factor to fluid and sheet parameters.[14] Brodkey[21] rewrote Dombrowski and John's[14] general dispersion equation in a clearer form

$$\beta_{i,\mathrm{nd}}^2 + \frac{(kh)^2}{Re_s}\beta_{i,\mathrm{nd}} + \frac{2(kh)^2}{We_s} - 2skh = 0 \tag{5}$$

where

$$\beta_{i,\mathrm{nd}} = \frac{\beta_i h}{U_s}, \qquad Re_s = \frac{U_s h}{\nu_l}, \qquad We_s = \frac{\rho_l U_s^2 h}{\sigma}$$

In the above equation, the first term represents the rate of change of momentum of a liquid element, the second term arises because of viscous effects, the third term represents the effect of surface forces, and the fourth term represents the effect of aerodynamic forces.

Weihs,[15] like Dombrowski and Johns,[14] stated that Kelvin-Helmholtz aerodynamic instabilities resulted in the breakup of a thin, viscous liquid sheet. However, Weihs[15] derived a general solution for the shape of the sheet by employing hypergeometric functions, which was subsequently simplified to apply to the far-field region (i.e., far from the nozzle, or the impingement point in this case), where changes in sheet thickness are negligible. He obtained the following equation for the growth rate factor:

$$\beta_i = \frac{\nu_l k^2}{2}\left[-1 + \sqrt{1 + \frac{8(\rho_g k U_s^2 - \sigma k^2)}{\nu_l^2 k^4 \rho_l h}}\right] \tag{6}$$

The same equation for the growth rate factor is obtained by reducing Dombrowski and Johns'[14] general dispersion equation [Eq. (5)].

Equation (6) relates β_i to the disturbance k for a given fluid, and sheet velocity. By differentiating β_i with respect to k, and setting the resulting expression equal to zero, the wave number of the fastest growing disturbance k_m can be found. Once k_m is known, the corresponding growth rate factor can be calculated using Eq. (6).

To predict drop-size characteristics, Dombrowski and Johns[14] reasoned that the sinusoidally-shaped sheet breaks into cylindrical ligaments at crest and trough points, and related d_L to the sheet thickness and wave number as

$$d_L = \sqrt{(4h/k_m)} \tag{7}$$

The ligaments subsequently break up into drops as a result of surface tension induced symmetrical wave growth. Dombrowski and Johns[14] assumed that the wave grows until the disturbance amplitude is equal to the ligament radius, thus resulting in one drop per wavelength. The drop size d_D for water in air is then

$$d_D = (3\pi/\sqrt{2})^{1/3} d_L[1 + (3\nu_l\rho_l/\sqrt{\rho_l \sigma d_L})]^{1/6} \approx 1.89 d_L \tag{8}$$

Taylor[7] made detailed measurements of the thickness and lateral spread of sheets formed by low-speed (<5.6 m/s) impinging water jets and noted[7,20] that the overall shape of the sheet was related to the presence of stationary antisymmetric waves within a limiting radius, which was defined as the radius where the Weber number based on local sheet thickness is unity. His measurements showed that h at any radial location r on the sheet was of the form $rh = F(\theta, \phi)$, which is independent of U_s. Hasson and Peck[22] used Taylor's[7] data to verify their analytically-derived expression for the sheet thickness

$$h = \frac{d_j^2 \sin^3\theta}{4r(1 - \cos\phi\cos\theta)^2} \tag{9}$$

Ibrahim and Przekwas[9] extended Taylor's[19] work to obtain an analytical solution for the shape of the sheet at low Weber numbers ($We < 500$), although for the high Weber number regime ($We > 2000$), they suggested the use of Weihs' analysis.[15] In the low Weber number regime, the authors suggested that stationary antisymmetric waves determine the shape of the sheet, which agrees with prior studies by Taylor[19] and Huang.[6] In the low Weber number regime, the expression for the sheet shape took the following form:

$$r_b = \frac{d_j h_o}{2h_e \sin\theta} \tag{10}$$

where r_b is the distance from the impingement point to the sheet edge, and h_o and h_e are the initial and edge sheet thicknesses, respectively. Details for calculating the initial and edge sheet thicknesses can be found in Ref. 9.

The semi-empirical theoretical models discussed above predict the sheet shape for the low Weber number regime, and the sheet breakup length and drop size for the high Weber number regime. These parameters form the basis for comparisons with the experimental results obtained in the present study.

Experimental Studies of Impinging Liquid Jets

Experimental studies on impinging injector systems have mainly been concerned with developing mean drop size and mixing efficiency correlations from cold flow measurements,[23-28] and under combusting conditions.[28] Studies that shed light on the important physical mechanisms controlling sheet breakup and subsequent drop-size formation have been less numerous[4-8]; important results from these studies are summarized below.

Heidmann et al.[4] performed an extensive experimental study on the atomization characteristics of two turbulent impinging jets as a function of d_o, L/d_o, l_j, U_j, 2θ, μ_l, and σ. From flash photographs, Heidmann et al.[4] identified four spray patterns. The first spray pattern, termed the closed rim regime, was characterized by a smooth liquid sheet surrounded by a thick rim that contained the major portion of liquid. This sheet pattern occurred at velocities below 4 m/s. The next observed spray pattern was the periodic drop pattern in which waves were evident on the sheet surface. In addition, drops detached tangentially off the sheet periphery at periodic intervals. The velocity range for this pattern was between 4–9 m/s. The open rim pattern, also observed between jet velocities of 4–9 m/s, was characterized by a thinning sheet, and unlike the closed rim pattern, the outside rim did not meet at the spray centerline. The last spray pattern identified was the fully developed pattern in which waves of drops were shed in a periodic

fashion from the sheet edge. Fully developed sprays were observed for jet velocities greater than 10 m/s. Heidmann et al.[4] also noted that there was a sharp transition between open rim and fully developed regimes.

In addition to identifying the four sheet patterns, Heidmann et al.[4] measured the shedding frequency of ligaments and drops from the edge of the sheet, and found that this "wave frequency" was linearly proportional to $U_j \cos \theta$. The wave frequency decreased with increasing impingement angle, while remaining relatively insensitive to changes in orifice diameter and preimpingement length. An important observation made in this study was the similarity between the measured wave frequency and the frequency of high-frequency instability modes observed in liquid rocket engines.[1,4]

Dombrowski and Hooper[5] performed an experimental study on turbulent and laminar impinging water jets. Dombrowski and Hooper[5] measured the sheet speed using high-speed cinematography and drop size from flash photographs as a function of jet velocity and impingement angle. Distinct sheet structure differences were seen between the laminar and turbulent impinging jet cases. The sheet formed from laminar impinging jets tended to produce much larger and smoother sheets as compared to the sheets formed by turbulent impinging jets. Measured sheet velocities tended to be between $U_j \cos \theta$ and U_j.

Dombrowski and Hooper[5] suggested that sheet breakup does not scale with Reynolds number, but is dependent on the jet velocity profile and impingement angle. For turbulent jets, "impact waves" formed at the impingement point disintegrated the sheet. For the laminar impinging jets, both impact waves and aerodynamic waves affected the sheet disintegration process. The authors[5] also stated that the wavelength of both impact waves and aerodynamic waves and the breakup length decrease with increasing jet velocity. However, breakup length measurements made from their photographs dispute the latter statement.

Huang[6] experimentally and analytically studied the breakup of liquid sheets formed by two opposing water jets ($2\theta = 180$ deg) injected through standard ASME sharp-edged orifices at jet velocities between 2–20 m/s. Huang[6] presented the measured nondimensional breakup radius $r_b/0.5d_o$ vs We, and indicated two Weber number-dependent breakup regimes connected by a transition regime.

In the first regime, $100 < We < 500$, the circular sheets were stable with a nearly perfect circular edge, and the nondimensionalized breakup radius increased with increasing Weber number. Huang[6] occasionally saw disturbances originating from the impingement point in this regime akin to the impact waves observed by Dombrowski and Hooper.[5] Huang[6] performed a force balance between the inertia and surface tension forces acting on the circular sheet to obtain an expression that related the nondimensional breakup radius to the Weber number (for $We < 900$).

The transition regime spanned a Weber number range from 500 to 2000. Huang[6] noted that cardioid waves emerged and predominated in part of this region ($500 < We < 800$). The nondimensional breakup radius reached a maximum between Weber numbers of 800–1000, and antisymmetric waves first appeared in this regime.

Huang[6] referred to the second breakup regime, $We > 2000$ (the maximum We for his experiments was 30,000), as the unstable liquid sheet regime where "the sheet flaps with a flag-like motion." In this regime, the nondimensional breakup radius decreased with increasing Weber number. Based on an analysis for a vibrating membrane, a semiempirical relation for the breakup radius was developed[6]

$$\left(\frac{r_b}{\frac{1}{2}d_o}\right) = 14.2s^{-2/3}We^{-1/3} \qquad (11)$$

Anderson et al.[8] investigated the spray characteristics of turbulent impinging jets by measuring the sheet breakup length x_b, W, and drop size as a function of flow velocity and injector geometry (2θ, d_o, L/d_o, and l_j). The experimental apparatus and the operating conditions of the impinging jet system were very similar to those of Heidmann et al.[4] In this study, the authors[8] found the breakup length to increase with decreasing impingement angle and increasing jet velocity, up to the maximum velocity tested (18.5 m/s), which agrees with observations made in previous experimental studies.[4] W was relatively independent of jet velocity and impingement angle. Changes in orifice L/d_o did not appreciably affect the spray characteristics, although variation in the preimpingement length l_j had a measurable effect on breakup length and drop size. Drop size and velocity measurements made with the phase Doppler particle analyzer (PDPA) at the spray centerline downstream of the impingement point showed the drop size decreasing with increasing jet velocity and increasing impingement angle, and that the drop velocity was nearly equal to the jet velocity. Analysis using linear stability theory provided predictions of drop size that reproduced the experimental trends, however, breakup length predictions did not follow the experimental trends.

Experimental

The atomization characteristics of two impinging water jets were experimentally evaluated using the experimental arrangement shown in Fig. 2, which is similar to that used by Heidmann et al.[4] and Dombrowski and Hooper,[5] and is essentially identical to that used by Anderson et al.[8] The experimental setup allowed for variation of the impingement angle and size (length and diameter) of the precision bore glass tubes. Precision bore glass tubes were utilized to minimize effects of surface roughness. Minor spatial adjustments to assure precise alignment of the impinging jets were provided by a micrometer stage mounted on one of the lines. The impinging jets were deemed to be aligned correctly when the plane including the two jets was visually observed to be normal to the plane of the resulting sheet. PDPA measurements in the spray field resulted in radial profiles of drop size that were symmetric about the centerline,[8] and showed that this simple procedure yields correct alignment. The flow system consisted of a 9.47-l (2.5-gal) tank filled with water pressurized by compressed nitrogen gas. The flow rate was monitored using rotameters, whereas the pressure drop across the glass tubes was measured using pressure gauges. Both turbulent and laminar impinging jets were studied. Experimental intricacies of each case are discussed below.

Turbulent Impinging Jets

Precision bore glass tubes were attached to 4.57-mm-i.d. (6.35-mm-o.d.) stainless steel tubes with fittings. The diameter and length of glass tubes used for the turbulent impinging jet experiments in this study were the same as those used by

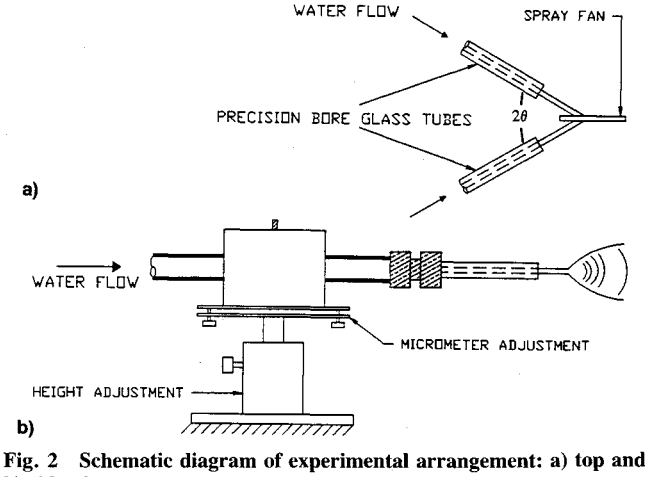

Fig. 2 Schematic diagram of experimental arrangement: a) top and b) side view.

Heidmann et al.[4] The tube orifice diameters were 0.64, 1.02, and 1.45 mm, whereas the length of the tubes was 50.8 mm; thus yielding a length-to-diameter ratio of 80, 50, and 35, respectively. The inlet of the glass tubes was sharp, and the ratios of fitting diameter (6.35 mm i.d.) to glass tube diameters were 9.92, 6.23, and 4.38, respectively. l_j for these turbulent impinging jet experiments was set to be 25.4 mm, thus yielding l_j/d_o, of 40, 25, and 18 for the three aforementioned tube geometries, respectively. Measurements were made at impingement angles, 2θ, of 40, 60, and 80 deg. The velocity of the water jets ranged between 5–20 m/s. The two water jets were turbulent since for all the velocities and diameters studied, the Reynolds number was greater than 2.3×10^3. In addition, no special contouring procedures were taken to ensure laminar flow, and the jet surface always appeared ruffled.

Instantaneous images of the spray field were taken using diffuse backlighting provided by a strobe light with a time duration of approximately 5 μs, while a CID solid state camera (512 by 512 pixels) was used to acquire the spray images. Typically, 17 spray images were obtained for each unique geometric and operating condition. From the spray images, the breakup length x_b, and the distance between any adjacent periodic structures λ, were measured. The breakup length was defined as the distance from the impingement point along the spray centerline to where the intact sheet disintegrates into ligaments and drops, which is the same definition given by Heidmann et al.[4] From the 17 spray realizations, the average value and corresponding standard deviation of the aforementioned measured parameters was obtained. High-velocity water jets emanating from small L/d_o tubes can lead to cavitation. For the cases presented here, no cavitation effects were observed. The cavitation number, defined as the ratio of the upstream pressure less the liquid's vapor pressure to the pressure drop across the orifice, was calculated for the various measurement conditions and compared with Nurick's critical cavitation number.[29] The cavitation behavior of the jets was found to be generally consistent with the results observed by Nurick[29] and is more fully discussed in Ref. 8.

Drop size and velocity measurements were made for the 0.64-mm-diam glass tube turbulent impinging jet case using an argon-ion (λ = 514.5 nm) laser-based, fast Fourier transform (FFT) version of the PDPA.[30,31] The theory behind the operation of the PDPA has been reviewed thoroughly in the literature,[30,31] hence, only a few system details are mentioned here. The collection optics were oriented 30 deg off axis from the forward propagation direction of the laser beam, which is the optimum angle for measuring transparent drops.[30] The optical configuration of the transmitting and collection optics chosen allowed the measurement drop-size range to span 40–1400 μm.

Drop size/velocity measurements for a set of parametric conditions were made in a previous study[8] at two locations downstream of the impingement point, x = 16 and 41 mm. At each downstream location, measurements were made at 6.4-mm increments in the plane of the sheet normal to the sheet centerline.[8] In this study, only the drop-size measurements at a single spatial location (x = 16 mm, along the sheet centerline) are presented as a function of jet velocity and impingement angle. At each measurement location, 8000 drops were measured, since at least 5500 data points are needed for $\pm 5\%$ accuracy in mean diameter measurements.[32]

Laminar Impinging Jets

A series of experiments involving laminar impinging jets was also undertaken using the experimental setup shown in Fig. 2. For these tests, 0.51-mm-diam precision bore glass tubes with an L/d_o ratio of 375 were used. The large L/d_o ratio ensures fully developed flow. These tubes are very similar to those used by Dombrowski and Hooper.[5] Each glass tube was attached to a 12.7-mm-o.d., 10.4-mm-i.d. brass tube with fittings. To ensure laminar flow through the precision bore glass tubes, an inlet glass tube was contoured such that the fluid transitioned smoothly from the brass tube to the glass tube. The transition angle between the inlet glass tube wall and the tube centerline was 17 deg. This contoured inlet tube was fused to the 0.51-mm-i.d. precision bore glass tube.

Contouring the inlet extended the Reynolds number range for laminar flow up to 1×10^4 as indicated by pressure drop measurements taken across the glass tube, and the glass-like appearance of the jets. Often, a "bursting phenomenon," attributed to velocity profile relaxation effects,[33] was observed where the smooth laminar jet would suddenly and violently turn chaotic at some distance from the tube exit.

As with the turbulent impinging jets, instantaneous images of the laminar impinging jet spray were taken using the CID camera and strobe light. Approximately 17 images at each operating and geometric condition were acquired from which the breakup length was measured. An average value and standard deviation of the measured quantity was determined and compared to model predictions and previous experimental studies.

Results and Discussion

The disintegration of sheets formed by two impinging liquid jets is modeled using two existing theories: 1) a stationary antisymmetric wave-based theory for low Weber numbers,[9] and 2) a linear stability-based theory for high Weber numbers.[8] The stationary antisymmetric wave-based theory yielded the shape of the sheet from which the breakup length was obtained, whereas the linear stability-based theory yielded breakup length and drop-size predictions. The breakup length predictions of both theories, and the drop-size predictions from the linear stability-based model are compared to experimental measurements. Breakup length measurements were made for both laminar and turbulent impinging jets, although drop-size measurements were made only for the turbulent impinging jet case. Finally, measurements of the distance between apparent wave-like structures on the sheet surface are presented for the turbulent impinging jet case as a function of jet velocity and orifice diameter.

General Spray Characteristics

The sheets typically produced by turbulent impinging water jets are shown in Fig. 3. Here, the orifice diameter was 0.64 mm and the jet velocities were 6.4 and 18.5 m/s. The freejet length prior to impingement, or l_j, was 25 mm, L/d_o was 80, and the impingement angle 2θ was 60 deg. The two instantaneous images shown in Fig. 3 fall into the fully developed regime identified by Heidmann et al.[4] It is interesting to note the apparent periodic nature of both the disturbances on the sheet surface and the detaching ligaments. Recall that Heidmann et al.[4] measured the wave frequency of detaching ligaments and drops and observed it to be linearly proportional to $U_j \cos\theta$.

Instantaneous images of sprays resulting from impinging laminar water jets are shown in Fig. 4. In this case, the orifice diameter was 0.51 mm, the jet velocities were 7.1 and 17.9 m/s, L/d_o was 375, the impingement angle was 60 deg, and l_j was approximately 10 mm. The images in Fig. 4 have the same scale as the images for the turbulent impinging jet case shown in Fig. 3. Despite the similarity between the operating and geometric parameters of the turbulent and laminar cases, the appearance of the sheets produced in each case is quite different. The sheets resulting from the impinging laminar jets are larger than their turbulent counterparts. In addition, the sheets for the laminar case tend to be much smoother and less chaotic. Dombrowski and Hooper[5] also observed distinct differences between turbulent and laminar impinging jet cases, and attributed these differences primarily to the different velocity profiles across the jets for the two cases. Dombrowski and Hooper[5] stated that impact waves originating from the impingement point were responsible for sheet disintegration for the turbulent impinging jet case as well as for the breakup of sheets formed by high-speed laminar impinging jets. These

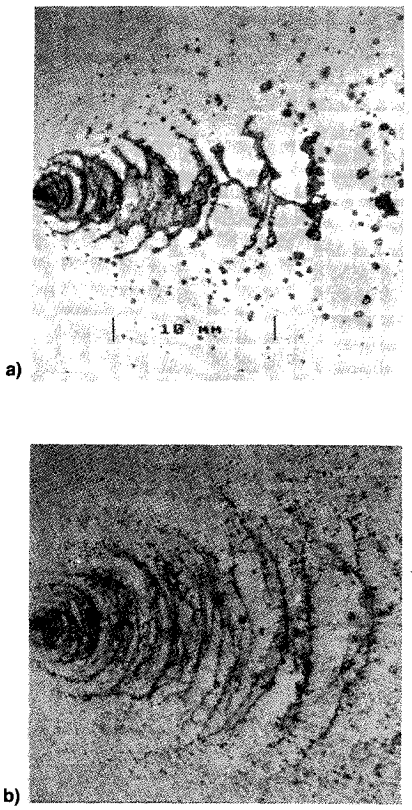

Fig. 3 Instantaneous images of sprays formed by two turbulent impinging water jets. The jets issued from 0.64-mm-i.d. L/d_o = 80 precision bore glass tubes. 2θ was 60 deg, while l_j was 25 mm. Flow is from left to right. U_j = a) 6.4 and b) 18.5 m/s.

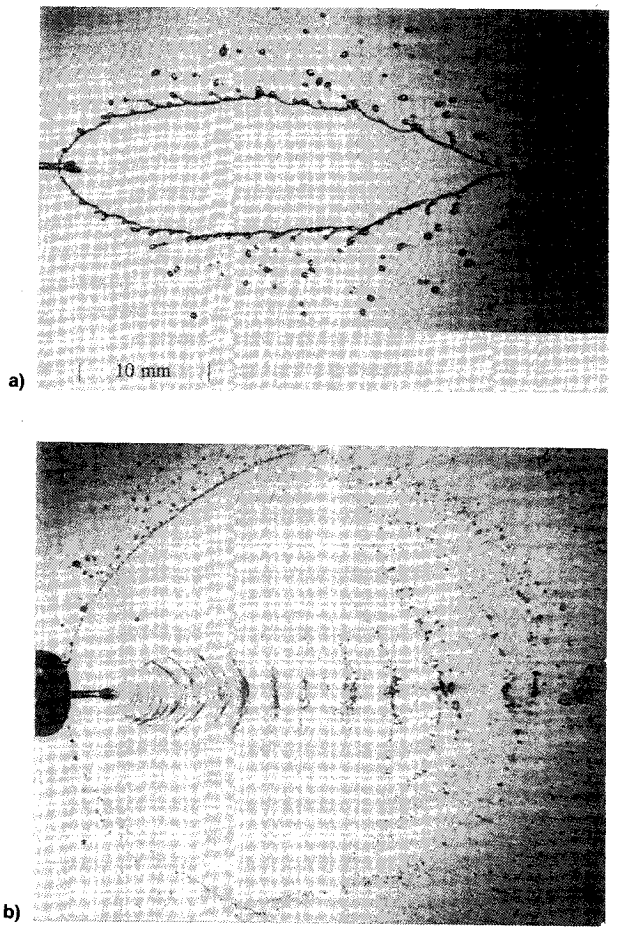

Fig. 4 Instantaneous images of sprays formed by two laminar impinging water jets. The jets emanated from 0.51-mm-i.d. L/d_o = 375 precision bore glass tubes. 2θ was 60 deg, while l_j was approximately 10 mm. Note that the scale of these images is the same as those in Fig. 3. In addition, the orifice diameter and jet velocities are similar for the images in both Fig. 3 and this figure. Flow is from left to right. U_j = a) 7.1 and b) 17.9 m/s.

impact waves can be seen in the U_j = 17.9 m/s image of Fig. 4, and appear to lead to the disintegration of the sheet. Careful inspection of the high-velocity case in Fig. 4 reveals tears at the center of the intact sheet as well. In addition, the impact waves are dominant in the center portion of the sheet. Dombrowski and Hooper[5] stated that the slower-moving fluid at the sheet periphery resulting from the laminar velocity profile across the jet tended to damp out the impact waves.

The images presented here demonstrate the importance of the jet condition prior to impingement in understanding the atomization process. The differences between laminar and turbulent impinging jet conditions involve details related to the velocity profile and turbulence intensity of the jets prior to impingement. Despite the clear importance of the jet's initial condition on the atomization process, no definitive studies presently exist to clearly differentiate velocity profile and turbulence intensity effects on atomization. Actual impinging injectors have small L/d_o values (typically less than five), and Re numbers which lie in the turbulent regime (typically 10^6). Thus, the velocity profiles developed under these short L/d_o ratios will not correspond to fully developed conditions. Furthermore, high-turbulence intensity levels are to be expected in actual conditions due to the flow-turning effects encountered in the injector manifold of typical rocket engines. The degree to which such phenomena control the atomization process remains a serious challenge to experimentalists and modelers interested in impinging jet injectors.

Analysis

The linear stability-based model was used to predict breakup length and drop size. For these predictions to be made, U_s must be known. Drop velocity measurements made in a previous study for turbulent impinging jets[8] indicated that for the entire tested velocity range (5–25 m/s), and impingement angle range (40 and 100 deg), the mean drop velocity was close to U_j. This result suggests that the sheet speed is the same as the speed of the incoming jets, U_j. Taylor[7] also noted that the jet and sheet speeds should be the same. Dombrowski and Hooper[5] measured the sheet speed through high-speed cinematography, and found essentially similar results for the sheet velocity. Consequently, U_s is assumed to be the same as U_j. In addition, it is assumed that d_j is the same as the orifice diameter d_o.

The first step taken was to compare Squire's[13] analysis with Dombrowski and Johns[14] and Weihs[15] analyses of viscous sheets. Weihs,[15] after simplifying his analysis, obtained the same expression relating the growth rate factor and wave number as Dombrowski and Johns.[14] Squire[13] provided explicit expressions for k_m [Eq. (3)] and $\beta_{i,m}$ [Eq. (4)] for the most unstable wave, which is assumed to control the breakup process of the liquid sheet. For the viscous sheets, the wave number of the most unstable wave k_m was found from Eq. (6), taken from Weihs' analysis.[15]

The wave number and growth rate factor of the fastest growing wave for both the viscous and inviscid cases were calculated and compared as a function of sheet velocity and sheet thickness for a water sheet in still air. With increasing sheet thickness and velocity, the maximum wave number predicted using the inviscid analysis becomes larger than that predicted by the viscous analysis. However, for the cases studied here, Squire's[13] simple expression for the wave number [Eq. (3)] of the most unstable wave results in less than 1% deviation from the viscous analysis results.

Furthermore, for the flow and geometric conditions of this study, $\beta_{i,m}$, predicted by the inviscid[13] and viscous[14,15] analyses, were also the same. However, for more viscous liquids

and higher gas densities (corresponding to higher chamber pressures), the two analyses will differ. Based on these observations, Squire's simple expressions for the wave number [Eq. (3)] and growth rate factor [Eq. (4)] of the most unstable wave were used to calculate breakup length and drop size.

The sheet breakup length is linked to the sheet velocity, disturbance growth rate, sheet thinning rate, and the ratio of the final to the initial disturbance amplitude. Recall that the breakup length is defined as the distance from the impingement point to where the intact sheet disintegrates along the spray centerline. The empirical relation given by Eq. (2) is used to compute x_b, using $\beta_{i,m}$ [see Eq. (4)], derived by Squire.[13] Inspection of Eq. (4) indicates the need for a sheet thickness expression. For the sheet thickness, Hasson and Peck's[22] expression [Eq. (9)] was used. With the three aforementioned equations, an explicit expression for x_b was derived as follows:

$$(x_b/d_o) = 5.451s^{-2/3}[Wef(\theta)]^{-1/3} \tag{12}$$

where d_o is the orifice diameter, and $f(\theta)$ is given as follows:

$$f(\theta) = [(1 - \cos\theta)^2/\sin^3\theta] \tag{13}$$

Note that the constant given by Eq. (13) is contained in the sheet thickness equation of Hasson and Peck[22] [Eq. (9)] for $\phi = 0$ deg (spray centerline). If a different expression for the sheet thickness was used, then $f(\theta)$ would have a different form. For conditions involving more viscous liquids and/or higher gas densities, the expression for β_i, for the viscous case given by Eq. (6) and Hasson and Peck's[22] sheet thickness relation [Eq. (9)], can also be used in conjunction with the empirical breakup relation [Eq. (2)]. The resulting expression could then be numerically integrated as a function of wave number to solve for the breakup length.[8]

Sheet Breakup Length Measurements

Sheet breakup length was calculated using Eq. (12), and compared to breakup length measurements made for both laminar and turbulent impinging jets. The numerical integration procedure outlined for the viscous case was also carried out and, as expected, the breakup length was identical to that predicted by Eq. (12). The nondimensional breakup length x_b/d_o is plotted as a function of the nondimensional scaling parameter $We(1 - \cos\theta)^2/\sin^3\theta$ in Fig. 5. For the experimental measurements, each symbol represents an average of 17 measurements, and the corresponding bars represent the ± standard deviations. The results obtained using linear stability-based theory collapse to a single line when plotted in the manner shown in Fig. 5. However, the measurements do not collapse in a similar fashion. Breakup length measurements for turbulent impinging water jets (d_o = 0.64 mm, L/d_o = 80) were made at discrete velocities of 6.4, 12.4, and 18.5 m/s, and at impingement angles of 40, 60, and 80 deg. For the laminar impinging jet case (d_o = 0.51 mm, L/d_o = 375), breakup length measurements were made at discrete velocities of 7.1, 13.3, and 17.9 m/s, and impingement angles of 40, 60, and 80 deg. It should be noted that different precision bore glass tubes used for the laminar cases sometimes led to different breakup length results. This measurement variability was likely due to small differences in tube inlets (i.e., transition angle), tube outlets, and internal surface conditions. The measurements were duplicated with several sets of glass tubes. The sensitivity of the sheet breakup process to apparently small variations in the tube characteristics for the laminar case reinforce the observation that the jet conditions strongly affect the spray formation process.

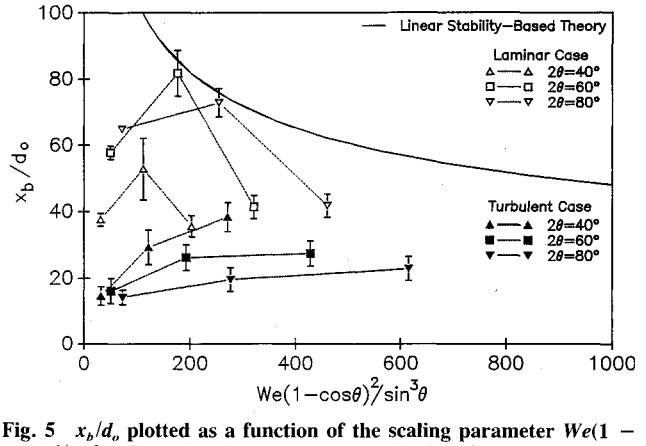

Fig. 5 x_b/d_o plotted as a function of the scaling parameter $We(1 - \cos\theta)^2/\sin^3\theta$. The solid line represents predictions made using linear stability-based theory. The solid symbols represent the turbulent impinging jet case measurements (d_o = 0.64 mm), whereas the hollow symbols represent the laminar impinging jet case measurements (d_o = 0.51 mm). Each point plotted represents the mean value of 17 separate measurements, and the bars indicate the ± standard deviation of the measurements for each measurement condition.

The predicted nondimensional breakup length decreases with an increase in the scaling parameter. However, the opposite trend is observed for the turbulent case measurements for all impingement angles. For the laminar impinging case, the nondimensional breakup length increases to a maximum, then decreases with increasing Weber number. The linear stability-based model also overpredicts the magnitude of the breakup length. However, the predicted breakup length magnitude can be altered by choosing a constant different than the one in Eq. (2).

Several conclusions can be drawn by comparing the laminar and turbulent impinging jet cases to each other as well as with the results of previous studies. For the turbulent impinging jet case, the breakup length decreases with increasing impingement angle, which is opposite to the general trend observed for the laminar jet case. Intuitively, the breakup length would be expected to increase with decreasing impingement angle since an increasing amount of momentum is directed in the axial direction and the sheet is thicker on the centerline. Dombrowski and Hooper[5] indicated that impact waves controlled the breakup of sheets formed by impinging turbulent jets, and that the breakup length would decrease with increasing jet velocity; this trend is not observed for the cases studied here. The opposing trend of breakup length as a function of impingement angle for the laminar and turbulent cases suggests that different breakup mechanisms are operative.

As mentioned previously, the breakup length increases to a maximum, then decreases for increasing Weber number for the laminar impinging jet case. Measurements showed that the largest breakup length typically occurred between Weber numbers of 550–725. Huang,[6] in his study of opposed impinging jets (2θ = 180 deg), showed that the breakup radius (or length) increased linearly to a maximum value and then decreased with increasing Weber number. The breakup radius reached a maximum between Weber numbers of 800–1000. For Huang's case of 2θ = 180 deg, the trigonometric term in the nondimensional scaling parameter $(1 - \cos\theta)^2/\sin^3\theta$ is one; therefore, his data for breakup radius increases linearly for the entire range of the abscissa shown in Fig. 5. However, direct comparisons between his results and the current data is clouded by the different jet conditions of the two sets of experiments. Huang[6] used sharp-edged ASME orifices, which indicates that the jet velocity profile was plug flow, and probably had low-turbulence intensity levels. Also, the equation derived by Huang[6] for breakup radius [Eq. (11)] ($We > 1000$) is similar to the equation derived here [Eq. (12)]. Inspection of the two equations shows that other than the constants, the exponents of both the We and s terms are identical. The constants differ because Huang[6] obtained the value for his constant by curve-fitting the equation to the data.

Dombrowski and Hooper[5] suggested that impact waves were responsible for sheet breakup for intermediate to high-speed laminar impinging jets, and for all but the lowest velocities

for turbulent impinging jets. This idea seems plausible since the breakup length for both the laminar and turbulent impinging jet cases approach similar values at high jet velocities (see Fig. 5). In addition, flash photographs of the sheets under the previously mentioned conditions indicate the presence of disturbances that appear to originate at the impingement point.

Ibrahim and Przekwas[9] proposed that their extension of Taylor's[19] stationary antisymmetric wave-based theory should be used in a low Weber number regime ($We < 500$), whereas linear stability theory should be applied to a high Weber number regime ($We > 2000$). In the low Weber number regime, the shape of the sheet is predicted using Eq. (10). The sheet shape predicted using the aforementioned equation is shown in Fig. 6 as a function of the impingement angle for an orifice diameter of 0.51 mm and a jet velocity of 7.1 m/s. Note that the impingement point is at $x = 0$, $y = 0$. The predicted sheet shape for $2\theta = 60$ deg looks similar to the corresponding image for the same conditions shown in Fig. 4 (low jet velocity case, $U_j = 7.1$ m/s). From the shape of the sheet, x_b can be obtained. The predicted sheet shapes have pointed tips, except for the opposed jet case ($2\theta = 180$ deg). For the laminar impinging jet case (experimental), sheets with pointed tips were observed for all impingement angles tested up to a Weber number of about 350. For Weber numbers greater than 350, the sheets disintegrated before a pointed tip was formed.

Further perusal of Fig. 6 indicates that the breakup length increases with increasing impingement angle up to about 100 deg, after which it decreases. However, the maximum sheet width increases with increasing impingement angle up to a maximum at $2\theta = 180$ deg. For the impingement angles studied in the present experiments ($2\theta = 40$, 60, and 80 deg) for the laminar impinging jet case, the general trend was for increasing breakup length with increasing impingement angle, the same trend predicted by the model. Since breakup length measurements were not made for impingement angles greater than 100 deg, the decrease in breakup length with increasing impingement angle for impingement angles greater than 100 deg as predicted by the model cannot be either confirmed or contradicted.

A comparison between the breakup length predicted by linear stability-based theory, Ibrahim and Przekwas'[9] extension of Taylor's[19] stationary antisymmetric wave theory, and the breakup length measurements for the laminar and turbulent cases is shown in Fig. 7. Specifically, x_b/d_o is plotted as a function of the nondimensional scaling parameter $We(1 - \cos\theta)^2/\sin^3\theta$, for an impingement angle of 60 deg. As seen

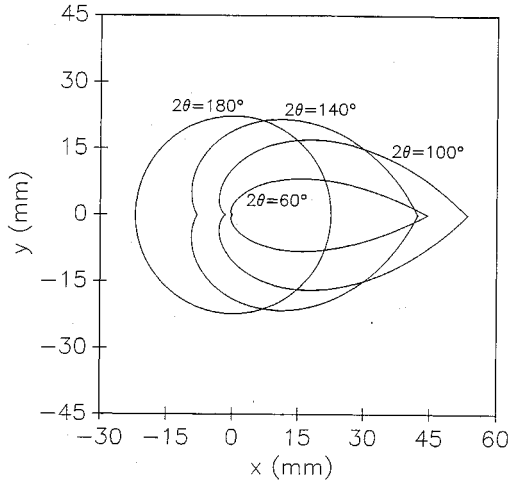

Fig. 6 Sheet shape predictions for water in air from the Ibrahim and Przekwas[9] model plotted as a function of impingement angle. The orifice diameter was 0.51 mm, and the jet velocity was 7.1 m/s. The predicted sheet shape for the 60-deg impingement angle case should be compared to the corresponding spray image (Fig. 4a). Note that the scales are different.

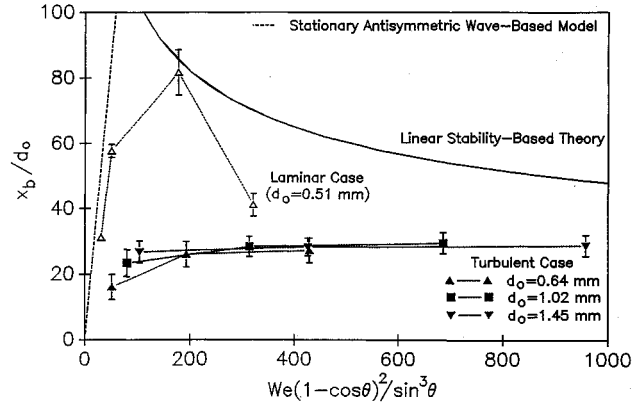

Fig. 7 x_b/d_o plotted as a function of the scaling parameter $We(1 - \cos\theta)^2\sin^3\theta$. The solid line represents predictions made using linear stability-based theory. The broken line represents breakup length predictions made using the stationary antisymmetric wave-based model for an impingement angle of 60 deg. The solid symbols represent the turbulent impinging jet case measurements, whereas the hollow symbols represent the laminar impinging jet case measurements. The experimental measurements shown are for a 2θ of 60 deg. Each point plotted represents the mean value of 17 separate measurements, and the bars indicate the ± standard deviation of the measurements of each measurement condition.

in Fig. 7, the breakup length as predicted by the Ibrahim and Przekwas[9] model is linearly proportional to Weber number, whereas for the linear stability-based model, it is proportional to $We^{-1/3}$. The breakup length predictions from the Ibrahim and Przekwas[9] model overpredict the breakup length measurements made for both the laminar and turbulent cases, however, the measured breakup length does increase with increasing Weber number, but not as strongly as the stationary antisymmetric wave-based model predicts. The model also predicts sheet shapes with pointed tips, as shown in Fig. 6. These sheets were only observed in the laminar impinging jet case for Weber numbers less than 350, which correspond to the first two data points for the laminar case in Fig. 7. As mentioned previously, the sheets formed by laminar impinging jets disintegrated before pointed tips were formed for Weber numbers greater than 350, thus explaining why longer sheets are predicted using the stationary antisymmetric wave-based model. For the turbulent impinging jet case, the measured nondimensional breakup lengths for various jet diameters lie on nearly a single curve for this fixed impingement angle. The same trend is observed at the other impingement angles, although different curves were observed for each angle. It should be noted that this collapse of the turbulent impinging jet results to a single curve for a fixed impingement angle is a reflection of the *We* number dependence, since the geometric factor in the nondimensional scaling factor remains constant for fixed impingement angle. Similar to Huang's[6] breakup radius results for opposed jets, and the present results for laminar impinging jets, it is likely that the breakup length for the turbulent impinging jet case will peak for some Weber number, and then decrease.

Drop-Size Measurements

Drop-size measurements using PDPA for the turbulent impinging jet cases were compared to predictions of the linear stability-based model. There are two models for calculating the drop diameter. The model proposed by Dombrowski and Johns[14] [Eqs. (7) and (8)] can be combined with Squire's[13] expression for the fastest growing wave number [Eq. (3)] and the nondimensional breakup length expression derived earlier [Eq. (12)], and recast in the following form:

$$(d_D/d_o) = [2.62/(12)^{1/3}]s^{-1/6}[Wef(\theta)]^{-1/3} \qquad (14)$$

where $f(\theta)$ is given by Eq. (13). The relationship shows that the ratio of the drop diameter to the orifice diameter has a

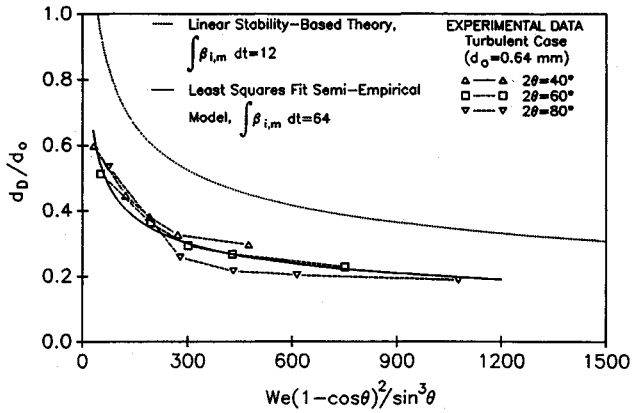

Fig. 8 d_D/d_o plotted as a function of a nondimensional scaling factor and impingement angle. Drop-size predictions made using linear stability-based theory and drop-size measurements made using the PDPA at an axial location of x = 16 mm, along the spray centerline y = 0, are shown.

weak inverse dependence on the scaling parameter $Wef(\theta)$. The second model, proposed by Ibrahim and Przekwas,[9] relates the drop size to k_m as

$$d_D = (\pi/k_m) \tag{15}$$

which can be recast as follows:

$$(d_D/d_o) = (2\pi\sigma/d_o\rho_g U_j^2) = (2\pi/sWe) \tag{16}$$

By contrasting the two relationships for the nondimensional drop diameter, it is evident that the former model shows a dependence on the impingement angle, whereas the latter model is independent of the impingement angle and inversely proportional to the *We* number.

The drop size measurements are compared with the linear stability-based model predictions [Eq. (14)] in Fig. 8. The drop size measurements shown in the figure are for a spatial location, x = 16 mm, along the sheet centerline. The abscissa in this figure is the nondimensional scaling parameter $Wef(\theta)$, whereas the ordinate is the drop diameter nondimensionalized with the orifice diameter. Note that the measured drop sizes are polydispersed, and the arithmetic mean diameter d_{10} is taken for comparison purposes. The theory predicts a monodispersed drop-size distribution. The comparison shows that the drop-size dependence on both the Weber number and the impingement angle is similar for both measurements and predictions. The nondimensionalization also brings the data for various impingement angles close to a single curve. It is not surprising that the measurements and theory do not match quantitatively, better agreement would be observed if a higher-order moment diameter, e.g., a d_{30}, for the measurements were used. Alternately, a larger empirical breakup constant (currently, $\int \beta_{i,m}\, dt = 12$) would bring the measurements and the model predictions closer. In this vein, an empirical breakup constant, $\int \beta_{i,m}\, dt = 64$, yields a semiempirical model of the form:

$$(d_D/d_o) = [2.62/(64)^{1/3}]s^{-1/6}[Wef(\theta)]^{-1/3} \tag{17}$$

that represents a least-squares fit to the measured d_{10}, as shown in Fig. 8. Finally, the use of the second drop-size model [Eq. (16)] predicts drop sizes that are an order of magnitude greater than those measured. Therefore, based on these observations, the former model for drop size has more merit.

Surface Wave Measurements

Heidmann et al.[4] measured the wave frequency of detaching ligaments and drops from the edge of the intact sheets formed by impinging jets as a function of operating and injector parameters. Two important results of their study[4] were that the wave frequency was linearly proportional to $U_j \cos\theta$, and the measured wave frequency closely matched the frequencies associated with observed combustion instability phenomena.

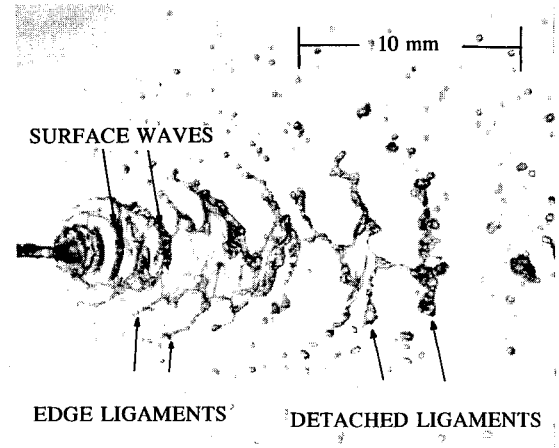

Fig. 9 Typical spray formed by two turbulent impinging water jets issuing from 0.64-mm-diam L/d_o = 80 glass tubes. The impingement angle was 60 deg, and the preimpingement length was 25 mm. Flow is from left to right. The distance between adjacent surface waves, edge ligaments, and detached ligaments were measured from such spray images.

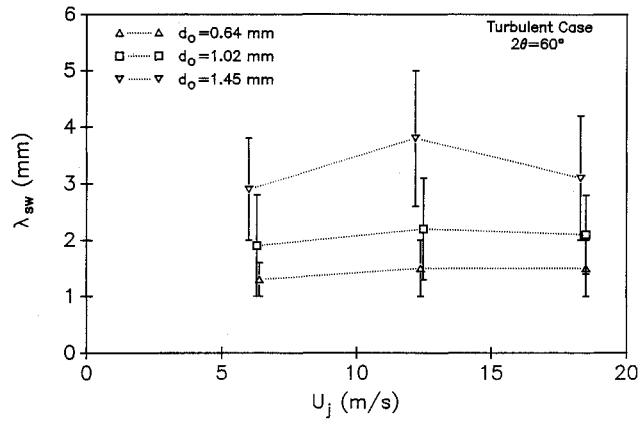

Fig. 10 Measured separation distance between adjacent surface waves λ_{sw} plotted as a function of jet velocity and orifice diameter for the turbulent impinging jet case at an impingement angle of 60 deg. Each point plotted represents an average between 10–50 separate measurements, while the corresponding bars indicate the associated standard deviation.

Because of the interesting results and the potential implications of the Heidmann et al.[4] study, similar measurements were made in this study. Specifically, for the turbulent impinging jet case, the distance between apparent adjacent periodic structures on and beyond the intact sheet surface were measured as a function of flow and injector characteristics. The types of periodic structures measured include surface waves, edge ligaments, and detached ligaments, all of which are shown in Fig. 9.

The surface wave category included disturbances on the intact sheet surface. Typically, the distance between adjacent surface waves λ_{sw} increased with increasing distance from the impingement point. Separation distance measurements were made over the entire intact sheet whenever possible to obtain an average λ_{sw}. The separation distance of adjacent surface waves is plotted as a function of jet velocity and orifice diameter for an impingement angle of 60 deg in Fig. 10. Each point plotted represents an average between 10–50 separate measurements, depending on operating conditions, while the corresponding bars represent the ± standard deviation. Despite the large standard deviation, there is a distinct increase

in λ_{sw} with increasing orifice diameter. However, for the cases studied, the separation distance was relatively insensitive to changes in jet velocity. Although not presented in graphical format, it was also found that the separation distance λ_{sw} was insensitive to changes in impingement angle.

Similar measurements were made for the edge and detached ligament categories. Edge ligaments were defined as strands of liquid attached to the intact sheet periphery. Detached ligaments were strands of fluid either completely or nearly completely separated from the downstream edge of the intact sheet. In general, the average separation distance between adjacent detached ligaments was larger than that of the edge ligaments. Likewise, the average separation distance between adjacent edge ligaments was larger than that of the surface waves. Again, the trends observed for λ_{sw} were also observed for the edge ligament category. The behavior of the separation distance between adjacent detached ligaments was not as apparent as the other two categories since not enough measurements were made to yield a meaningful average and standard deviation. It is interesting to note that the measured separation distances of the surface waves and edge ligaments are similar in magnitude to the fastest growing wavelength predicted by Squire[13]:

$$\lambda_m = (4\pi\sigma/\rho_g U_s^2) \tag{18}$$

However, the wavelength of the most unstable wave predicted by Eq. (18) is strongly dependent on sheet velocity and independent of the orifice diameter. This is contrary to the observed behavior of the various measured separation distances.

Summary and Conclusions

A systematic study of the atomization of impinging liquid jets investigating the effects of jet conditions (laminar vs turbulent), orifice diameter, impingement angle, and jet velocity has been conducted. Results of the present study have been compared to current theories in terms of sheet breakup length, drop size, and sheet shape. Experiments contrasting laminar and turbulent jet conditions clearly demonstrate that the jet conditions have a dramatic effect on the atomization process. Specifically, the measured breakup lengths for the laminar impinging jet case are longer and displayed different trends as a function of jet velocity and impingement angle than those of the turbulent impinging jet case. The present results are in complete agreement with earlier studies by Dombrowski and Hooper[5] with regards to the effects of jet conditions on impinging jet atomization. These results encourage speculation that velocity profile and turbulence characteristics of the jets strongly affect the atomization processes for impinging jet injectors. However, quantitative assessment of the specific mechanisms controlling atomization remain to be established.

For low Weber number ($We < 350$) laminar impinging jet conditions, predictions based on stationary antisymmetric wave-based theory were within 50% of the observed breakup length. Comparisons were also made with a linear stability-based theory. The linear stability-based theory predicted a monotonically decreasing sheet breakup length with increasing Weber number, which is opposite to the trend observed for turbulent impinging jets. In fact, experimental observations for both the laminar and turbulent jets argue strongly for the impact wave theory put forward by Dombrowski and Hooper[5] as the operative mechanism leading to sheet breakup. Thus, the current use of linear stability-based theories for describing sheet breakup for impinging jet conditions appears to be questionable for the range of conditions investigated in this study. In contrast, the linear stability-based theory provided reasonable predictive capability for drop size with respect to the trends observed for increasing Weber number and impingement angle. Measurements regarding the surface wave and periodic ligament formation for the turbulent jet studies indicate that the observed wavelengths are directly proportional to the orifice diameter and independent of jet velocity and impingement angle.

Based on the results of the present study, approaches to modeling impinging jet atomization should focus on including the impact wave process identified by Dombrowski and Hooper,[5] which none of the current models treat. Periodic perturbations associated with the jet inertia at the impingement region are often argued to be the likely mechanism for generating impact waves. A fundamental mechanistic model for the generation and growth of impact waves and their association with the subsequent atomization process is currently lacking. Additionally, the relationship between the periodic surface wave and ligament structures observed in the present work needs to be considered in light of their potential to initiate and sustain combustion instability phenomena associated with impinging jet rocket injectors.

Acknowledgments

The authors would like to thank David Grupp and Gayle Ramdeen for their assistance in carrying out the laminar impinging jet studies, and Doug Smith for his assistance in fabricating the glass tubes used in the laminar impinging jet experiments. The authors would also like to acknowledge the support of the Air Force Office of Scientific Research, Air Force Systems Command, USAF under grant number AFOSR 91-0336, as well as the support of the Penn State NASA Propulsion Engineering Research Center under Grant NAGW 1356. The U.S. Government is authorized to reproduce and distribute reprints for government purposes notwithstanding any copyright notation thereon.

References

[1]Anderson, W. E., Ryan, H. M., and Santoro, R. J., "Combustion Instability Phenomena of Importance to Liquid Bi-Propellant Rocket Engines," 28th JANNAF Combustion Meeting, San Antonio, TX, Oct.–Nov. 1991.

[2]Claflin, S. E., and Volkman, J. C., "Oxygen/Hydrogen Micro-Orifice Impinging Injector Development for Modular Test Chambers," *Propulsion Engineering Research Center Fourth Annual Symposium*, Huntsville, AL, 1992, pp. 53–58.

[3]*Liquid Propellant Rocket Instability*, edited by D. T. Harrje and F. H. Reardon, NASA SP-194, 1972.

[4]Heidmann, M. F., Priem, R. J., and Humphrey, J. C., "A Study of Sprays Formed by Two Impinging Jets," NACA TN 3835, March 1957.

[5]Dombrowski, N., and Hooper, P. C., "A Study of the Sprays Formed by Impinging Jets in Laminar and Turbulent Flow," *Journal of Fluid Mechanics*, Vol. 18, Pt. 3, 1963, pp. 392–400.

[6]Huang, J. C. P., "The Breakup of Axisymmetric Liquid Sheets," *Journal of Fluid Mechanics*, Vol. 43, Pt. 2, 1970, pp. 305–319.

[7]Taylor, G. I., "Formation of Thin Flat Sheets of Water," *Proceedings of the Royal Society of London, Series A: Mathematical and Physical Sciences*, Vol. 259, No. 1296, 1960, pp. 1–17.

[8]Anderson, W. E., Ryan, H. M., Pal, S., and Santoro, R. J., "Fundamental Studies of Impinging Liquid Jets," AIAA Paper 92-0458, Jan. 1992.

[9]Ibrahim, E. A., and Przekwas, A. J., "Impinging Jets Atomization," *Physics of Fluids A*, Vol. 3, No. 12, 1991, pp. 2981–2987.

[10]Childs, R. E., and Mansour, N. N., "Simulation of Fundamental Atomization Mechanisms in Fuel Sprays," *Journal of Propulsion*, Vol. 5, No. 6, 1989, pp. 641–649.

[11]Rangel, R. H., and Sirignano, W. A., "Nonlinear Growth of Kelvin-Helmholtz Instability: Effect of Surface Tension and Density Ratio," *Physics of Fluids*, Vol. 31, No. 7, 1988, pp. 1845–1855.

[12]Rangel, R., and Hess, C., "Nonlinear Spacial Instability of a Fluid Sheet," AIAA Paper 90-0118, Jan. 1990.

[13]Squire, H. B., "Investigation of the Instability of a Moving Liquid Film," *British Journal of Applied Physics*, Vol. 4, No. 6, 1953, pp. 167–169.

[14]Dombrowski, N., and Johns, W. R., "The Aerodynamic Instability and Disintegration of Viscous Liquid Sheets," *Chemical Engineering Science*, Vol. 18, No. 3, 1963, pp. 203–214.

[15]Weihs, D., "Stability of Thin, Radially Moving Liquid Sheets," *Journal of Fluid Mechanics*, Vol. 87, Pt. 2, 1978, pp. 289–298.

[16]Levich, V. G., *Physicochemical Hydrodynamics*, Prentice-Hall,

Englewood Cliffs, NJ, 1962, Chap. 11.

[17]Li, X., and Tankin, R. S., "On the Temporal Instability of a Two-Dimensional Viscous Liquid Sheet," *Journal of Fluid Mechanics*, Vol. 226, 1991, pp. 425–443.

[18]Lin, S. P., Lian, Z. W., and Creighton, B. J., "Absolute and Convective Instability of a Liquid Sheet," *Journal of Fluid Mechanics*, Vol. 220, 1990, pp. 673–689.

[19]Taylor, G. I., "The Dynamics of Thin Sheets of Fluid II. Waves on Fluid Sheets," *Proceedings of the Royal Society of London, Series A: Mathematical and Physical Sciences*, Vol. 253, No. 1274, 1959, pp. 296–312.

[20]Taylor, G. I., "The Dynamics of Thin Sheets of Fluid III. Disintegration of Fluid Sheets," *Proceedings of the Royal Society of London, Series A: Mathematical and Physical Sciences*, Vol. 253, No. 1274, 1959, pp. 313–321.

[21]Brodkey, R. S., *Phenomena of Fluid Motions*, Addison-Wesley Series in Chemical Engineering, Reading, MA, 1967.

[22]Hasson, D., and Peck, R. E., "Thickness Distribution in a Sheet Formed by Impinging Jets," *AIChE Journal*, Vol. 10, No. 5, 1964, pp. 752–754.

[23]Ferrenberg, A., Hunt, K., and Duesberg, J., "Atomization and Mixing Study," Contract NAS8-34504, Dec. 1985.

[24]Rupe, J. H., "Experimental Studies of the Hydrodynamics of Liquid Propellant Injection," Jet Propulsion Lab., California Inst. of Technology, External Publication 388, Pasadena, CA, June 1957.

[25]Vassallo, P., Ashgriz, N., and Boorady, F. A., "Effect of Flow Rate on the Spray Characteristics of Impinging Water Jets," *Journal of Propulsion and Power*, Vol. 8, No. 5, 1992, pp. 980–986.

[26]Hautman, D. J., "Spray Characterization of Like-on-Like Doublet Impinging Rocket Injectors," AIAA Paper 91-0687, Jan. 1991.

[27]Knight, R. M., and Nurick, W. H., "Interim Report, Correlation of Spray Drop Size Distribution and Injector Variables," NASA CR NAS7-726, Sept. 1969.

[28]George, D. J., "Rocket Injector Hot Firing and Cold Flow Spray Fields," AIAA Paper 73-1192, Nov. 1973.

[29]Nurick, W. H., "Orifice Cavitation and Its Effects on Spray Mixing," *Journal of Fluids Engineering*, Dec. 1976, pp. 681–687.

[30]Bachalo, W. D., and Houser, M. J., "Phase/Doppler Spray Analyzer for Simultaneous Measurement of Drop Size and Velocity Distributions," *Optical Engineering*, Vol. 23, No. 5, 1984, pp. 583–590.

[31]Ibrahim, K. M., Werthimer, G. D., and Bachalo, W. D., "Signal Processing Considerations for Laser Doppler and Phase Doppler Applications," *Applications of Laser Techniques to Fluid Mechanics*, edited by R. J. Adrian, D. F. G. Durão, F. Durst, M. Maeda, and J. H. Whitelaw, Springer-Verlag, New York, 1991, pp. 291–316.

[32]Lefebvre,, A. H., *Atomization and Sprays*, Hemisphere, Philadelphia, PA, 1989, p. 370.

[33]Lefebvre, A. H., *Atomization and Sprays*, Hemisphere, Philadelphia, PA, 1989, pp. 45–48.